The 2018 World Congress on
Advances in Civil, Environmental, & Materials Research (ACEM18)
Songdo Convensia, Incheon, Korea, August 27 - 31, 2018

Control of the VIV of a cantilevered square prism with free-end suction

Li Shiqing[1)], Wang Hanfeng[2)] and Peng Si[3)]

[1), 2), 3)] *School of civil engineering, Central South University, Changsha, China*
[2)] wanghf@csu.edu.cn

ABSTRACT

A steady slot suction near the free-end leading edge of a finite-length square cylinder was used to control its aerodynamic forces and vortex-induced vibration (VIV) . The aspect ratio (*H/d*, where *H* and *d* are the height and width of the cylinder, respectively) of the tested cylinder is 5. The tested suction ratio *Q*, which is defined as the ratio of suction velocity (U_s) over the oncoming flow velocity at which the strongest vibration occurs (U_v), ranged from 0 to 3. It was found that the RMS value of the VIV amplitude reduces quickly with the increase of *Q* from 0 to 1, then keep approximately constant with $Q \geq 1$.The maximum reduction of the VIV occurs at $Q = 1$, with the vibration amplutide reduces by 92% relative to the uncontrol case.

1. Introduction

Vortex-induced vibration (VIV) has long been the subject of fundamental and engineering investigations, it is also a classic fluid-structure interaction phenomenon, especially the VIV of a two-dimensional cylinder. Our understanding on the VIV of 2D cylinder has been significantly deepened in the last two decades, which has been sumarrized in the review articles, e.g. Chen et al. (1995); Khalak & Williamson (1996); Cheng et al. (2003); Jauvtis & Williamson (2003); Sarpkaya (2004); Williamson & Govardhan (2004); Gabbai & Benaroya (2005); Williamson & Govardhan (2008); Bearman (2011), etc.

For an 2D circular cylinder, VIV occurs when the vortexs shedding requency matches with one of the natural frequencies of the cylinder. The amplitude of VIV is closely related to mass-damping ratio ($m^*\zeta$) (Khalak & Williamson 1996; Khalak & Williamson 1997) and Reynolds number (*Re*) (Raghavan & Bernitsas 2011), where m^* is mass ratio and ζ is damping ratio, respectively. Additionally, the mass ratio is also a vital parameter which determines both the branches of resonance (Initial Branch, Upper branch, Lower branch), and the region of excitation, etc (Feng 1968; Khalak &

[1), 3)] Graduate Student
[2)] Professor

Williamson 1997). The near wake behind an oscillating cylinder is also a long established field of study. Up to now, four modes of vortex formation, including 2S mode, 2P mode, 2C mode and 2T mode, have been observed, e.g. Williamson & Roshko (1988); Williamson & Jauvtis (2004); Flemming & Williamson (2005), etc.

The diversified methods used to control the forces or VIV of 2D and three-dimensional (3D) bluff bodies can be generally classified into passive and active. For 2D cylinder, a number of control methods have been suggested to suppress the VIVs, including a moving wall (Wu et al. 2007), a momentum injection (Modi 1997), a dynamic burst control plate (Grager et al. 2011), synthetic jets (GIezer & Amitay 2002), etc.

Actually, a lot of structures in engineering applications are finite in length or height, such as high-rise buildings and cooling towers. Under the effects of finite span, wall junction and free end, the flow around a wall-mounted finite-length structure is highly 3D and different drastically from that around a nominal 2D one. However, relevant papers about the VIV and flow control for finite-length cylinders are far less than those for 2D bluff bodies, which is not conductive to our understanding.

In wind engineering, outer shape optimization for a high-rise building is one of the typical applications of passive flow control. To reduce the wind load and flow induced vibration (FIV) of high-rise building, shape optimization, such as corner rounding, chamfering, recession and slotted opening, etc. are widely used (Tanaka et al. 2012, Mooneghi & Kargarmoakhar 2016, Elshaer et al. 2017). Recently, active control methods have also been applied for suppressing the aerodynamic forces of simplified models of high-rise buildings. Menicovich et al. (2014) proposed an active flow control approach to improve the aerodynamic performance of a simplified building model with a rectangular cross section. They found steady tangential blowing positioned near the spanwise leading edge of the model can cause a reduction in the mean and fluctuating aerodynamic forces.

Apparently, since the spanwise shear flow of a 3D cylinder bears obvious similarities to that of the corresponding 2D cylinder, the control methods for the later are presumably still applicable for the former. Considering that the free-end shear flow of a 3D cylinder connects the spanwise shear flow from its both sides (Wang & Zhou 2009, Kawai et al. 2012), the nature of the free-end shear flow may have remarkable effects on the entire near wake, especially for the cylinders with relative small *H/d*.

By now, it is still not clear whether the VIV of a cantilevered cylinder can be controlled by manipulating its free end shear flow. The present paper reports an experimental investigation on this topic. A steady slot suction near the leading edge of the free end of a finite-length square cylinder was utilized to suppress the free-end shear flow and control the VIV of the cylinder. The effect of suction ratio (*Q*) on the control results was also studied systematically.

2. Experimental details

2.1 Experimental setup

The experiments were conducted in an open-loop wind tunnel with a 1000 mm long square test section of 450 mm by 450 mm. The maximum flow velocity in this test section is 40 m/s, and the longitudinal turbulence intensity is less than 0.5%. A

finite-length square cylinder with d of 40 mm and effective H/d of 5 was flexiblely installed through the bottom wall of the test section. As shown in figure 1(a), the x, y and z axes were in the streamwise, lateral and spanwise directions, respectively. The blockage ratio caused by the model was about 3.9%, whose effects were neglected in the following discussions. During the experiments, the freestream oncoming flow velocity (U_∞) was from 3.8~12.8 m/s, the corresponding Reynolds number (= $U_\infty d/\nu$, where v is the kinematic viscosity of air) was form 10400 to 35000. Relative to a structure with curved surface, e.g. circular cylinder, the aerodynamic characteristics of a finite-length square cylinder with H/d = 5 are less sensitive to the effects of Reynolds number (Wang et al. 2017). Thus, the main findings and conclusions of the present investigation may be also applicable at higher Reynolds numbers.

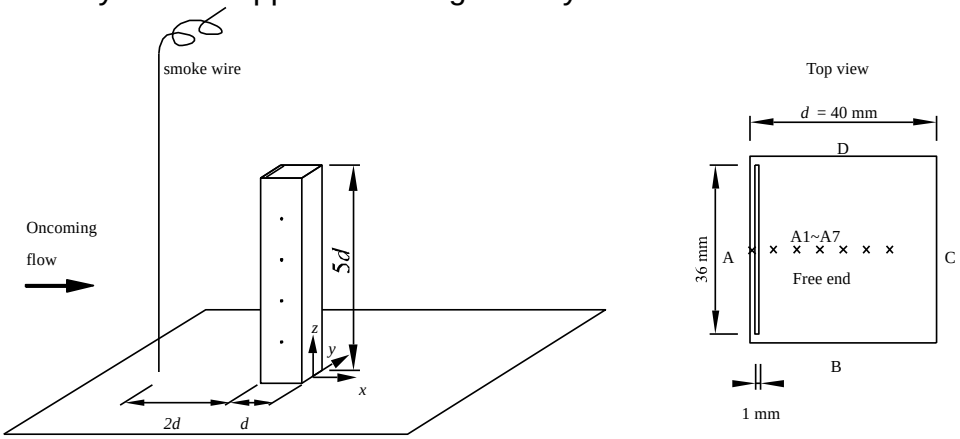

Figure 1 schematic of the experimental setup and the coordinate system

The tested model was made of acrylonitrile butadiene styrene (ABS) resins with 3D printing technique. The thickness of the four lateral walls of the model is 2 mm. The model penetrated through the bottom wall of the wind tunnel, fixed with a cantilever steel sheet, which is also penetrated into the model. The damping ratio of the cylinder is 0.7%, and the mass ratio is 250. The natural frequency of the model is 11.37 Hz. The suction slot was located at the free end, 1 mm (0.025d) downstream from its leading edge, as shown in figure 1. The total length of the slot was 36 mm (0.9d), and the width was 1 mm (0.025d). To manipulate the free end shear layer, a steady suction was established at the slot using a vacuum pump located outside of the test section. The flow rate of the vacuum pump was monitored with a volume flow meter. Consequently, the mean suction velocity (U_S) at the slot could be calculated based on the mean volume flow rate and the area of the slot. The power of the vacuum pump could be adjusted continuously to control U_S. The suction ratio Q, defined as U_S/U_∞, was varied from 0 to 3 in the present experiments, to test its effects on the control results, and the suction velocity was quite uniform along the whole length.

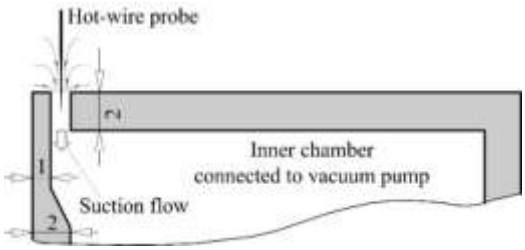

Figure 2 arrangement of hot-wire to document the suction flow.

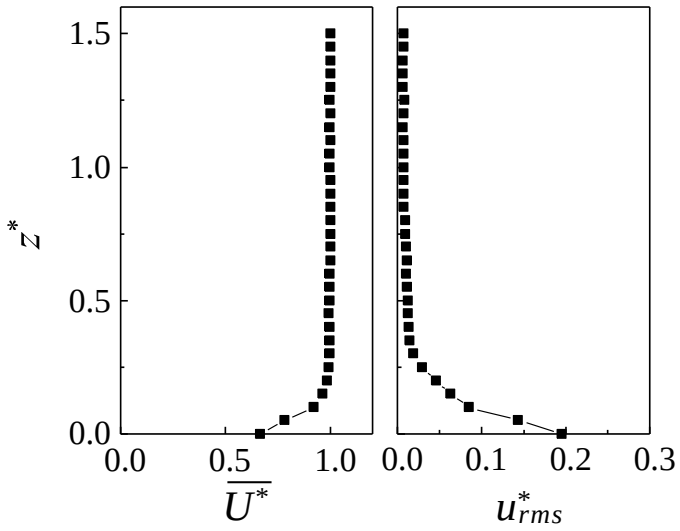

Figure 3 Distribution of $\overline{U^*}$ and u^*_{rms} in the boundary layer on the bottom wall.

The boundary layer on the wind tunnel bottom wall was documented using a Cobra probe (TFI, Series 100) at the position of the cylinder axis prior to its installation. The sampling frequency of the Cobra probe was 2 kHz, and the sampling duration for each measurement point was 20 s. The measurement uncertainty of a Cobra probe depends largely on the resolution of its built-in pressure transducer. For the present experiments, the uncertainty were estimated to be about ±4 and ±8 % for $\overline{U^*}$ and u^*_{rms}, i.e. the time-averaged streamwise velocity and the root-mean-square value of the stremwise fluctuation velocity, respectively. The superscript "*" in the present paper indicates normalization with U_∞ and/or d. Figure 3 presents the distributions of $\overline{U^*}$ and u^*_{rms} on the bottom wall. The boundary layer thickness was about 0.25 d. That is, most of the cylinder span was in uniform oncoming flow with the turbulence intensity of approximately 0.5%.

2.2 Measurement techniques

The pressure distribution was measured at four spanwise locations, i.e. z^* = 1, 2, 3, 4, to monitor the three-dimensional aerodynamic forces. At each spanwise location, there were 2 pressure taps distributed uniformly around the cylinder, with 1 taps on each faces. Each tap was connected to one channel of the pressure sensors (CYY4) using a PVC tube with the length of about 25 cm and inner diameter of 0.6 mm. The sampling frequency of the pressure scanner was 2000 Hz/channel. A total of 20,000 samples were collected for each channel.

Time-averaged pressure coefficient $\overline{C_p}$ and fluctuation pressure coefficient C_{p_rms} are defined as $\overline{C_p} = 2(\bar{P}-P_\infty)/\rho U_\infty^2$ and $C_{p\_rms} = 2P_{rms}/\rho U_\infty^2$, where $\bar{P}$ is the time-averaged pressure at each tap, P_{rms} is the root-mean-square value of the fluctuation pressure, P_∞ is the static pressure of the wind tunnel. The over bar "¯" denotes time-average in the present paper. Both P_∞ and P_d were also measured by two channels of the pressure scanner connected to a pitot tube placed in the wind tunnel. The sectional fluctuating lift coefficient C'_{lz}, were obtained based on the integration of the pressure measurement results at $z^* = 1, 2, 3, 4$. Moreover, the overall fluctuating lift coefficient C'_{lz} of the tested cylinder could be estimated by the weighted average values of the five sectional results along the span using Eq. (1):

$$C'_{lz} = (1.5C'_{lz}+C'_{lz}+C'_{lz}+1.5C'_{lz}) / 5 \quad (1)$$

A Cobra probe was used to document the characteristics of the free-end shear flow at different Q, to reveal the effects of the slot suction on it. In the present experiment, the measurements were conducted along z direction at seven locations, i.e. A1 to A7, along the centerline of the free end, as marked by "×" in figure 1. The first measurement location A1 was 0.5 mm downstream from the leading edge of the free end. A1 was upstream from the suction slot, as shown in Figure 1(a). The spacing between two adjacent measurement locations was 5 mm. For each measurement point in the free-end shear flow, the sampling frequency of the Cobra probe was 2 KHz, and the sampling duration was 30 s.

Flow visualization was also performed using smoke-wire technique for the free-end shear flow to reveal its transition at different Q. The smoke-wire was placed about $2d$ upstream from the tested cylinder. Smoke was generated with silicon oil coated on the smoke-wire heating by a pulse current. The flow visualization was conducted at $U_\infty \approx 1.1$ m/s, corresponding to the Reynolds number of 3000. The flow visualization images were then taken by a Cannon 6D SLR camera synchronized with the pulse current.

3. Results and discussions

3.1 Amplitude

The normalized maximum RMS values of tip across-wind displacements(A^*_{max}) of the cylinder with different Q are presented in Figure 4, which are used to evaluate the influence of the free-end suction on VIV. For the uncontrolled case (Q = 0), the presented A^*_{max} is 0.12, then The A^*_{max} decreases noticeably with the increase of Q from 0 to 1. For $Q \geq 1$, these values keep approximately constant. Obviously, the minimum of A^*_{max} presents at Q = 1, corresponding to the maximal reduction, relative to the uncontrolled case (Q = 0), of 92%. Correspondingly, the prism kept still, which shown that the VIV was almost completely suppressed.

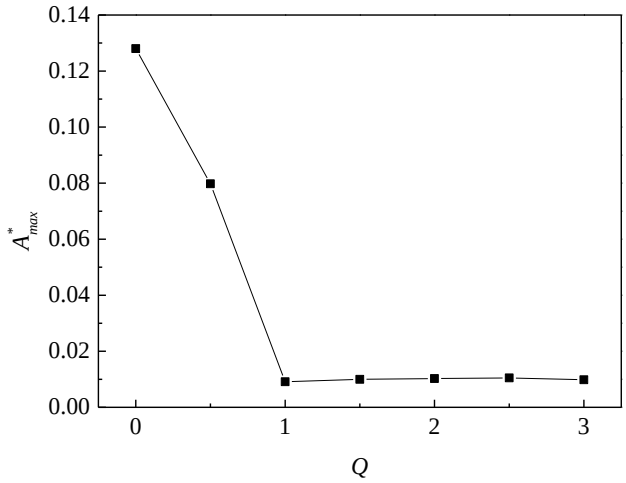

Figure 4. Dependence of the A*max on *Q*.

To highlight the effects of free-end suction on the suppression of VIV at Q = 1, figure 5 gives normalized RMS values of tip across-wind displacements (A^*) of the prism with different reduced wind speeds (U/f_0d) at Q = 0 and Q = 1.

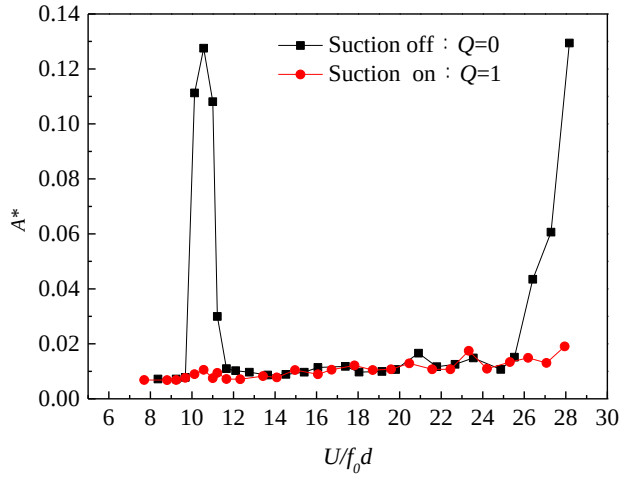

Figure 5. Reduced rms amplitude of VIV versus reduced velocity.

Starting from rest, the tip across-wind displacements of the square prism were measured for reduced velocity ranging from 8 up to 28. For reduced velocity below 9.8 no significant oscillation occurs at Q = 0. For reduced velocity ranging from 9.8 up to 12, a typical VIV amplitude response can be observed, meanwhile the maximum oscillation amplitude occurs at a reduced velocity close to 11. At higher reduced velocity galloping oscillations appear which are not studied here. At Q = 1, the normalized RMS values of tip across-wind displacements for reduced velocity ranging from 8 up to 28 are always close to 0.01, which shown that the prism was almost completely still.

3.2 Fluctuating lift

Figure 6 shows the variation of the fluctuating lift (C_l') of the tested finite-length cylinder with the increase of Q. For the uncontrolled case (Q = 0), the present measured

C_l' is 0.48, then the C_l' decrease noticeably with the increase of Q from 0 to 1, corresponding to the reduction of amplitudes. For $Q \geq 1$, the fluctuation lift coefficients keep approximately constant. Obviously, the minimum of C_l' also present at Q = 1, corresponding to the maximal reduction of amplitude, relative to the uncontrolled case (Q = 0), of 87%. This variation explains why the amplitude of VIV at Q = 1 (suction on) is far smaller than that of Q = 0 (suction off).

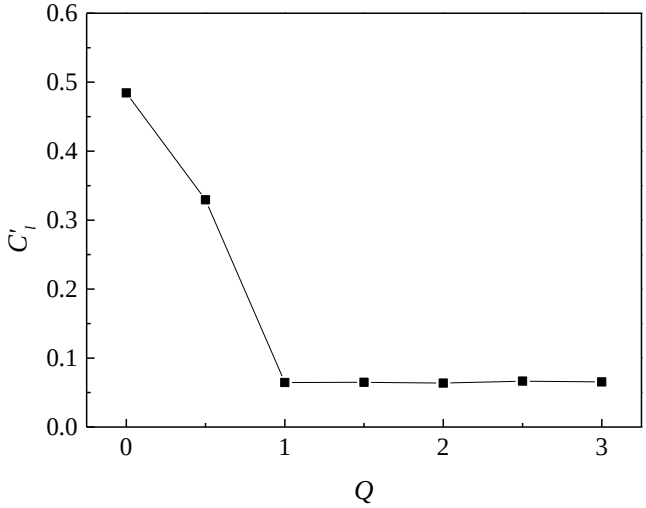

Figure 6 Dependence of the overall fluctuating lift coefficient C_l' on Q.

It is interesting to know the effects of free-end suction on the local fluctuating lift at different spanwise positions, since the flow around a wall-mounted finite-length cylinder is highly three dimensional. Figure 7 presents the sectional fluctuating lift coefficients C_{lz}' along the cylinder span at different Q, ranged from 0 to 3. For the uncontrolled case, although most of the cylinder span is immersed in uniform oncoming flow (see figure 2), C_{lz}' is not constant along the cylinder span. The C_l' is the smallest at z^* = 4 and increases gradually with the bottom wall approached. The downwash flow tends to attenuate spanwise vortex shedding and convert it from anti-symmetric to symmetric (Wang et al. 2006), thus resulting in smaller fluctuation lift. The effect of downwash flow retreats with decreasing z^* (departing from the free end), which leads to the gradually increase of C_{lz}' with the bottom wall approached. For the controlled case with $Q \geq 1$, C_{lz}' at all measured spanwise positions is smaller than the uncontrolled case. The maximum reduction of C_{lz}' occurs at $Q \geq 1$, and the reduction rates of C_l' at z^* = 4, 3, 2 and 1 are always higher than 80%. It is interesting to note that, the free-end suction suppresses C_l' not only near the free end, but also over the entire cylinder span. This observation suggests that the slot suction which manipulates the free-end shear flow can change the whole near wake flow and the aerodynamic forces over the entire cylinder span, then suppress the VIV.

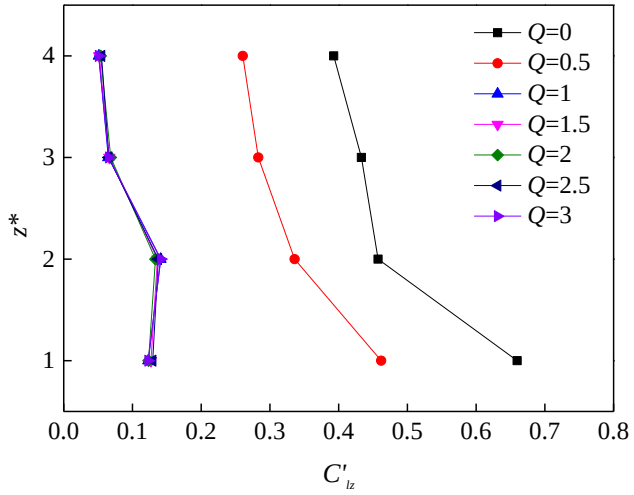

Figure 7 Sectional fluctuating lift coefficients along the cylinder span.

3.3 Free-end shear flow

Figure 8 shows the flow visualization results of the near wake flow in the symmetric plane at $y^* = 0$. It is worth emphasizing than it's very difficult to document the characteristics of the free-end shear flow on a oscillating prism by a cobra probe, so the measurement was done in the case of another prism, which fixed with four 6 mm stainless steel bolts. The magnification of the free-end shear flow is also given in figure 8 (c) for $Q = 1$. The solid red lines in figure 8 (a & b) indicates the shape of shear layer. Note that, the suction ratios are calculated based on U_∞ of 1.1 m/s, which is used for the flow visualization experiments.

For the uncontrolled case, the shear flow separates from the free-end leading edge and overshoots the cylinder. This shear flow bends towards the ground and forms a downwash at about 2*d* downstream from the cylinder. This downwash flow interacts with the spanwise shear flow in the near wake, resulting in the special aerodynamic characteristics of a finite-length cylinder (Tamura and Miyagi 1999, Wang et al. 2017).

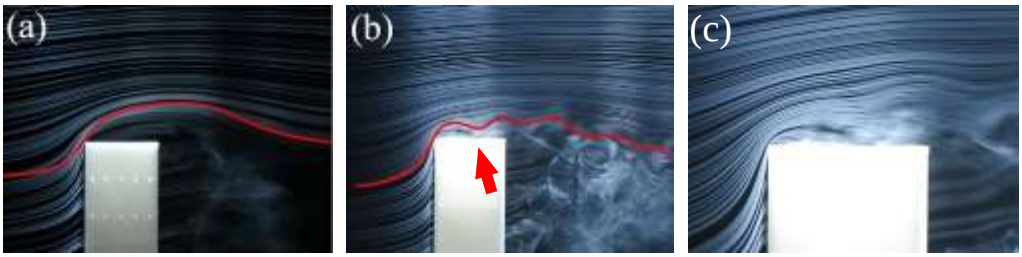

Figure 8 Flow visualization of the free-end shear flow at Re = 3000, (a) $Q = 0$, (b & c) $Q = 1$. The red arrow indicates the position of re-attachment.

For the controlled case with $Q = 1$, the free-end shear flow separates at the leading edge and reattaches on it at approximately 0.5*d* downstream (figure 8c), forming a recirculation bubble on the free end. It is observed that, the free-end shear flow becomes quite unstable under the effect of leading edge suction, which is characterized by a wavy motion as moving downstream (figure 8b). This wavy free-end shear flow may

interact more violently with the spanwise vortices relative to that of the uncontrolled case.

The distribution of mean streamwise velocity $\overline{U^*}$ and turbulent kinetic energy (TKE) of the free-end shear flow measured at the positions of A1 - A7 (see figure 1) are shown in figure 9 for Q = 0 and 1. The definition of TKE is given in Eq. (2), in which u'^2, v'^2 and w'^2 are the variances of the fluctuation velocities in x, y and z directions, respectively.

$$\text{TKE} = \frac{u'^2 + v'^2 + w'^2}{2U_\infty^{*2}} \tag{2}$$

Note that, the effective measurement range of a Cobra probe is a corn area with the apex angle of 90º with the accuracy of ± 1 m/s. It is not capable of identifying reversed flow (Crouch et al. 2014; Bell et al. 2016). An indication of the percentage of flow that is outside its calibrated cone of acceptance is provided by the software. In the present experiments, once this acceptance ratio is lower than 80%, the result at that point will be omitted. Taking the uncontrolled case as an example, there are some data absent at the measurement points adjacent to the free end, which can be apparently ascribed to the highly angled or recirculating flow in the separated region on the free end (Sumner et al. 2004). The shape of this region corresponds well with the shear layer revealed by the flow visualization, as shown in figure 8(a). In the case with Q = 1, the region of the separated flow shrinks significantly compared with that in Q = 0. The separated flow reattaches on the free end at the position approximately between A5 and A6 (as shown in figure 9a), forming a recirculation bubble. Again, this observation consists with that shown in figure 8(c).

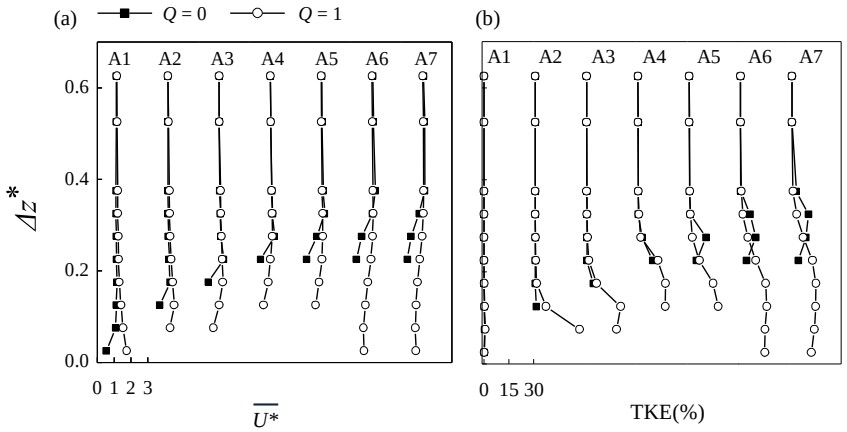

Figure 9 Distribution of $\overline{U^*}$ and TKE over the cylinder free end.

For the cases with Q = 1, a clear streamwise acceleration can be observation in the boundary layer at the position of A1, i.e. the leading edge of free end, as shown in figure 9. This tangential acceleration is very similar to the mean acceleration effect of a plasma actuator used for flow control over an airfoil, which transfers high momentum fluid across the shear layer and forces it to attach on the surface (Nishiri & Wygnanshi 1998, Greenblatt et al. 2012). The present acceleration observed at A1 in figure 9(a) can be ascribed to the slot suction which removes the low speed fluid immediately behind the free-end leading edge. Thus, the high momentum fluid, which originally tends to

separate from the leading edge, replenishes the low momentum fluid removed by the slot suction.

The TKE measurement result shown in figure 9(b) indicates the strength of momentum transport in the flow over the cylinder free end. At the position of A1, the TKE is approximately zero for all tested suction ratios except for Q = 1 at very close to the free end. At the positions from A2 to A7, i.e. downstream from the suction slot, the difference of the TKE distribution becomes significant for the three typical Q. For the case with Q = 1, the maximum TKE is obviously lager than that of the uncontrolled case. Moreover, the location where the maximum TKE occurs is much closer to the free end relative to the uncontrolled case. This observation agrees very well with that revealed by the flow visualization, as shown in figure 9(a & b). The strong turbulent fluctuation generated at Q = 1 may enhance the momentum transport between the high momentum outer flow and the wake, thus induces stronger downwash and suppress the spanwise vortex shedding more effectively relative to uncontrolled case.

4. Conclusions

The present paper proposes a novel aerodynamic control method with steady suction at its free end, to mitigate the VIV of high-rise buildings. A finite-length square cylinder with H/d = 5 was used as a simplified high-rise building model. A steady slot suction near the leading edge of the free end is utilized to manipulate the free-end shear flow and to control the fluctuation lift on the cylinder. The tested suction ratio Q, defined as the ratio of the suction velocity at the slot to the oncoming velocity, ranges from 0 to 3. Based on the experimental investigation, the following conclusions can be drawn:

(1) Steady free-end slot suction can significantly suppress the overall fluctuation lift of the finite-length square cylinder. Relative to the uncontrolled case, the overall fluctuation lift decrease with Q increasing from 0 to 1. The maximum reduction of C_l' are 87%, which occurs at Q = 1. At $Q \geq 1$, the reduction rate of the local fluctuating lift (C_{lz}') at z^* = 4, 3, 2 and 1 are always higher than 80%. It suggests the steady slot suction suppresses the aerodynamic forces not only near the cylinder free end but also over the entire cylinder span.

(2) Steady free-end slot suction can significantly suppress the VIV of the finite-length square prism. The normalized maximum RMS values of displacements at the top of the model (A^*_{max}) reduce quickly with the increase of Q from 0 to 1, then keep approximately constant with $Q \geq 1$.The maximum reduction of the the maximum RMS value occurs at Q=1, which reaches 92%.

(3) The free-end shear flow is sensitive to the slot suction near the leading edge. For the uncontrolled case, the oncoming flow separates at the leading edge and overshoots the free end. At Q = 1, the oncoming flow reattaches on the free end forming a recirculation bubble. The TKE of the flow over the free end is the highest at Q = 1, which may result in the strongest mixing of the high momentum shear flow and the near wake. Consequently, the slot suction with Q = 1 suppresses the spanwise vortex shedding more effectively and results in smaller fluctuation lift and amplitudes of VIV.

Acknowledgement

The authors wish to acknowledge support given to them from NSFC through Grants 11472312.

References

Bearman, P. W. (2011). Circular cylinder wakes and vortex-induced vibrations. Journal of Fluids & Structures, 27(5), 648-658.
Bell, J.R., Burton, D., Thompson, M.C., Herbst, A.H. & Sheridan, J., 2016 Dynamics of trailing vortices in the wake of a generic high-speed train. J. Fluids Struct. 65, 238-256.
Chen, S. S., Zhu, S., & Cai, Y. (1995). An unsteady flow theory for vortex-induced vibration. Journal of Sound & Vibration, 184(1), 73-92.
Cheng, L., Zhou, Y., & Zhang, M. M. (2003). Perturbed interaction between vortex shedding and induced vibration. Journal of Fluids & Structures, 17(7), 887-901.
Choi, H.C., Jeon, W.P. & Kim, J.S., 2008 Control of flow over a bluff body. Annu. Rev. Fluid Mech. 40: 113-139.
Crouch, T.N., Burton, D., Brown, N.A.T., Thompson, M.C. & Sheridan, J. 2014 Flow topology in the wake of a cyclist and its effect on aerodynamic drag. J Fluid Mech. 748, 5-35.
Elshaer, A., Bitsuamlak, G. & Damatty, A., 2017 Enhancing wind performance of tall buildings using corner aerodynamic optimization. Eng. Struc., 136: 133-148.
Feng, C. C. 1968 The measurement of vortex induced ef fects in flow past stationary and oscillating circular and D-section cylinders . Master's thesis , University of British Columbia , Vancouver , B . C ., Canada .
Flemming, F., & Williamson, C. H. K. (2005). Vortex-induced vibrations of a pivoted cylinder. Journal of Fluid Mechanics, 522(522), 215-252.
Gabbai, R. D., & Benaroya, H. (2005). An overview of modeling and experiments of vortex-induced vibration of circular cylinders. Journal of Sound & Vibration, 282(3–5), 575-616.
Greenblatt, D., Schneider, T. & Schule, C.Y., 2012 Mechanism of flow separation control using plasma actuation. Physics of Fluids 24, 077102.
Glezer A, Amitay M (2002) Synthetic jets. Annu Rev Fluid Mech, 34:503–529.
Grager T, Rothmayer A, Hu H (2011) Stall suppression of a low-Reynolds-number airfoil with a dynamic burst control plate. In: 49th AIAA aerospace sciences meeting including the new horizons forum and aerospace exposition, AIAA 2011–1180, Orlando, FL.
Jauvtis, N., & Williamson, C. H. K. (2003). Vortex-induced vibration of a cylinder with two degrees of freedom. Journal of Fluids & Structures, 17(7), 1035-1042.
Kawai, H., Okuda, Y. & Ohashi, M., 2012. Near wake structure behind a 3D square prism with the aspect ratio of 2.7 in a shallow boundary layer flow. J. Wind Eng. Ind. Aerodyn. 104-106(3), 196-202.
Khalak, A., & Williamson, C. H. K. (1997). Investigation of relative effects of mass and damping in vortex-induced vibration of a circular cylinder. Journal of Wind Engineering & Industrial Aerodynamics, s 69–71(97), 341-350.
Khalak, A., & Williamson, C. H. K. (1997). Fluid forces and dynamics of a hydroelastic structure with very low mass and damping. Journal of Fluids & Structures, 11(8),

973-982.
Khalak, A., & Williamson, C. H. K. (1999). Motions, forces and mode transitions in vortex-induced vibrations at low mass-damping. Journal of Fluids & Structures, 13(7-8), 813-851.
Menicovich, D., Lander, D., Vollen, J., Amitay, M., letchford, C. & Dyson, A., 2014 Improving aerodynamic performance of tall buildings using Fluid based Aerodynamic Modification. J. Wind Eng. Ind. Aerodyn., 133: 263-273.
Modi VJ (1997) Moving surface boundary-layer control: a review. J Fluids Struct 11:627–663.
Mooneghi, M.A. & Kargarmoakhar, R., 2016 Aerodynamic Mitigation and Shape Optimization of Buildings. Review. J. Building Eng., 6: 225-235.
Nishri, B. & Wygnanski I., 1998 Effects of periodic excitation on turbulent separation from a flap. AIAA J. 36(4), 547-556.
Raghavan, K., & Bernitsas, M. M. (2011). Experimental investigation of reynolds number effect on vortex induced vibration of rigid circular cylinder on elastic supports. Ocean Engineering, 38(5–6), 719-731.
Sarpkaya, T. (2004). A critical review of the intrinsic nature of vortex-induced vibrations. Journal of Fluids & Structures, 19(4), 389-447.
Summer, D., Heseltine, J.L. & Dansereau, O.J P., 2004 Wake structure of a finite circular cylinder of small aspect ratio. Exp. Fluids 37, 720–730.
Tamura, T. & Miyagi, T., 1999 The effect of turbulence on aerodynamic forces on a square cylinder with various corner shapes. J. Wind Eng. Ind. Aerodyn. 83, 135-145.
Tanaka, H., Tamura, Y., Ohtake, K., Nakai, M. & Kim, Y.C., 2012 Experimental investigation of aerodynamic forces and wind pressures acting on tall buildings with various unconventional configurations. J. Wind Eng. Ind. Aerodyn., 107-108: 179-191.
Wang, H.F., Zhao, X.Y., He, X.H. & Zhou, Y., 2017 Effects of oncoming flow conditions on the aerodynamic forces on a cantilevered square cylinder. J. Fluids Struct. 75: 140-157.
Wang, H.F. & Zhou, Y., 2009 The finite length square cylinder near wake. J. Fluid Mechanics, 638: 453-490.
Wang, H.F., Zhou, Y., Chan, C.K. & Lam, K.S., 2006 Effect of initial conditions on interaction between a boundary layer and a wall-mounted finite-length-cylinder wake. Phys. Fluids 18: 065106.
Williamson, C., & Roshko, A. (1988). Vortex formation in the wake of an oscillating cylinder. Journal of Fluids & Structures, 2(4), 355-381.
Williamson, C. H. K., & Jauvtis, N. (2004). A high-amplitude 2t mode of vortex-induced vibration for a light body in xy ja:math, motion. European Journal of Mechanics, 23(1), 107-114.
Williamson, C. H. K., & Govardhan, R. (2004). Vortex-induced vibrations. Annu.rev.fluid Mech, 36(1), 413-455.
Williamson, C. H. K., & Govardhan, R. (2008). A brief review of recent results in vortex-induced vibrations. Journal of Wind Engineering & Industrial Aerodynamics, 96(6–7), 713-735.
Wu, C. J., Wang, L., & Wu, J. Z. (2007). Suppression of the von kármán vortex street behind a circular cylinder by a travelling wave generated by a flexible surface. Journal of Fluid Mechanics, 574(574), 365-391.